Ladder climbing and multiphoton dissociation of polyatomic molecules excited with short pulses: Basic theory and applications to HCO

Peter Schwendner, Christian Beck, and Reinhard Schinke
Max-Planck-Institut für Strömungsforschung, D-37073 Göttingen, Germany
(Received 11 February 1998)

We present a numerically efficient algorithm for multiphoton dissociation of molecules with light pulses in the infrared frequency regime. The shape of the external electric field can be arbitrary. The method is essentially based on discretizing the continuum; dissociation is simulated by a coordinate-dependent cutoff function. A substantial reduction of the computer time required for solving the large set of first-order differential equations in time ($N \approx 2000$) can be achieved if the interaction with the field can be separated according to $\hat{W}(t) = E(t)\hat{\mu}_{\text{eff}}$, where $\hat{\mu}_{\text{eff}}$ is an effective coordinate-dependent dipole moment function. We applied this method to the excitation and dissociation of the triatomic molecule HCO including all three vibrational degrees of freedom. Comparison with calculations based on the propagation of a wave packet on a three-dimensional grid yields good agreement, provided the rate of excitation is not too large. The accuracy of classical trajectory calculations is also tested. [S1050-2947(98)04907-5]

PACS number(s): 33.80.Wz

I. INTRODUCTION

The interaction of a molecule with light is one of the most fundamental processes in physics and chemistry [1]. If the intensity of the electromagnetic field is weak and if the light source is operated under continuous-wave (cw) conditions, the interaction can be described by first-order perturbation theory and more or less simple expressions for, e.g., the population transfer from the initial to a final state as a function of time or the absorption cross section can be derived [2,3]. The situation becomes more complicated, however, when the light pulse is comparably short and/or when the intensity is high. Under such conditions, first-order perturbation theory breaks down and either higher-order treatments must be applied [4] or the time-dependent Schrödinger equation including the molecule-field interaction has to be solved without any further approximations [5].

A topic that has attracted a great deal of research activities, is the dissociation of molecules through the absorption of several photons in the infrared regime [6–9]. In the past, experiments were performed with cw lasers, and the degree to which the resonance condition was fulfilled, i.e., the frequency of the laser had to be very close to one of the fundamental frequencies of the molecule, essentially determined the rate of excitation and subsequent dissociation. Today it is possible to generate intense laser pulses in the infrared regime with pulse lengths well below 1 ps [10,11]. These new technologies allow one to perform studies that were previously not possible or at least very difficult. For example, in a recent experiment Maas *et al.* [12] observed excitation of NO up to the fifth excited vibrational level when it is exposed to a 150 fs infrared pulse. An obvious question is, how does the efficiency of this process depend on the ''internal ladder'' of the free molecule or the parameters of the pulse such as intensity, frequency, or duration?

Ladder climbing in molecules with more than one vibrational degree of freedom offers even more interesting questions to be tackled. Is the ladder climbing process mode specific or does it progress in a more statistical manner? What happens when the molecule reaches an energy regime where the dynamics is irregular (or classically chaotic)? Does the excitation process terminate because the coupling between levels diminishes or does the dissociation rate increase, because the resonance condition is better and better fulfilled as a consequence of the increased density of vibrational states? In which way does internal energy redistribution influence the excitation process? How is the absorbed energy distributed among the various degrees of freedom of the products?

The present paper is the first in a series of publications in which we will investigate ladder climbing and dissociation in small polyatomic molecules such as HCO or HNO. The internal dynamics of these molecules is well understood and therefore they are ideally suited to investigate their response to strong external fields. Moreover, they are sufficiently small to allow a rigorous numerical treatment without the use of approximations. In the present paper we outline the basic numerical tools, present some of the results for HCO, and discuss these results in terms of the characteristic features of this simple molecule. More applications will be published elsewhere.

II. METHODS OF CALCULATIONS

In the following, $\hat{H}_0$ specifies the time-independent Hamiltonian of the free molecule and the corresponding stationary eigenfunctions are denoted by ψ_i with energies E_i. The interaction with the electric field is described semiclassically, i.e., $\hat{W}(t) = -\vec{E}(t)\cdot\vec{\mu}$, where $\vec{\mu}$ is the coordinate-dependent dipole-moment vector and $\vec{E}(t)$ is the time-dependent electric field vector. The excitation of the molecule through the coupling with the external field is determined by the time-dependent Schrödinger equation

$$i\frac{\partial}{\partial t}\Phi(t) = [\hat{H}_0 + \hat{W}(t)]\Phi(t); \tag{1}$$

the explicit dependence of the wave function on the internal coordinates of the molecule is suppressed in order to simplify notation. The initial condition for the wave function is $\Phi(t)=\psi_i$ when initially the molecule was in the ith state.

One way of solving Eq. (1) is the direct propagation of $\Phi(t)$ on a suitable multidimensional grid [13]. This method is numerically exact provided the mesh size is sufficiently small. Furthermore, it is rather general and can be used for, in principle, arbitrary fields $\vec{E}(t)$ [14]. Ample examples of grid propagations have been reported in the literature [15] (see also the exquisite review by Manz for a comprehensive list of references [16]). However, there is one severe drawback, namely the computer time increases quickly with each additional vibrational degree of freedom. Especially if the pulse duration is long (>1 ps), the computation time may be too long for obtaining converged results. As a consequence, there are actually only very few applications for systems with more than two modes [17–22]. Despite the exceedingly long computer times, a few ''exact'' calculations on a grid have been performed by us and the results will be presented in Sec. IV; details will be given below. Because of these purely technical problems, wide variations of the pulse parameters are basically prohibited for all practical purposes. However, the grid calculations can be utilized for testing an alternative but approximate method, which is considerably faster.

If *all* the eigenfunctions of the molecular Hamiltonian are known, an expansion of the time-dependent wave function according to

$$\Phi(t)=\sum_i c_i(t)\psi_i \tag{2}$$

is computationally more convenient than propagation of the wave packet on a grid, provided the number of states is not unmanageably large. Inserting Eq. (2) into the Schrödinger equation and utilizing the orthonormality of the ψ_i leads to the well known set of first-order differential equations,

$$i\frac{d}{dt}\underline{c}(t)=[\underline{\underline{H}}_0+\underline{\underline{W}}(t)]\underline{c}(t), \tag{3}$$

where $\underline{\underline{H}}_0$ is a diagonal matrix with elements $H_{ii'}=E_i\delta_{ii'}$. (In what follows, underbars indicate vectors and double underbars indicate matrices.) The coupling matrix is given by

$$\underline{\underline{W}}(t)=-\vec{E}(t)\cdot\underline{\underline{\vec{\mu}}}, \tag{4}$$

with the elements of the dipole moment matrix being defined by $\vec{\mu}_{ii'}=\langle\psi_i|\vec{\mu}|\psi_{i'}\rangle$. The initial conditions for the expansion coefficients read $c_i(t)=\delta_{ii'}$. In the following we will refer to the expansion of the wave function in terms of the eigenfunctions as the *matrix method* in contrast to the *grid method* mentioned above.

The matrix method is completely analogous to a grid propagation provided only the bound states of $\hat{H}_0$ are excited. However, if the molecule absorbs more and more photons, the mean molecular energy gradually approaches the dissociation threshold and eventually the molecule can dissociate. In order to allow for the rupture of one of the bonds, one has to include also continuum states in the expansion basis. There are, however, two basic problems. First, the calculation of continuum wave functions, although possible even for a triatomic molecule [23], is computationally very demanding. Second, there are in principle infinitely many continuum states.

In the present work we proceed in the following way. First, we artificially hinder the molecule to dissociate by placing an infinitely high barrier at some value of the dissociation coordinate, $R_{\max}$. This distance must be sufficiently large to warrant that the molecule practically is dissociated when the bond distance has reached this value. Subsequently, we calculate the bound states of the free molecule within this multidimensional ''box'' and include all of them up to some maximum energy $E_{\rm cut}$ in the basis. By shifting the boundary to larger distances, one can decrease the mean energy spacing between the ''discretized'' continuum states. In the limit that $R_{\max}$ approaches infinity, the number of basis functions also becomes infinite and this procedure would be exact. Of course, that is impossible.

Since all basis functions are confined to the box, the molecule cannot dissociate. In order to simulate dissociation, we use the same trick as is employed in normal grid calculations; they are also performed on a finite grid and therefore cannot represent dissociation. After every time step the evolving wave packet is multiplied by a coordinate-dependent split function $f_{\rm split}$. This function is equal to one in the inner region of the potential, where the bound states are localized, and smoothly diminishes towards the end of the grid [24]. Its purpose is to suppress those parts of the evolving wave packet that approach the border of the finite grid as the time is increased from t to $t+\Delta t$. Without this function the wave packet would reappear at the other side of the grid and thus lead to spurious numerical effects.

In the matrix propagation scheme we proceed in an equivalent way. Multiplication of the wave packet with a coordinate-dependent function $f_{\rm split}$ corresponds to multiplying—from the left—the coefficient vector $\underline{c}(t)$ with the matrix $\underline{\underline{f}}$ having elements

$$f_{ii'}=\langle\psi_i|f_{\rm split}|\psi_{i'}\rangle. \tag{5}$$

Because $f_{\rm split}$ is one in the region over which the true bound-state wave functions extend, $f_{ii'}=\delta_{ii'}$ for the true bound states. The element is zero if one state is a true bound state and the other one is a discretized continuum state. However, when both wave functions are discretized continuum states, $f_{ii'}$ is different from zero. Thus, the matrix $\underline{\underline{f}}$ has the following structure:

$$\underline{\underline{f}}=\begin{pmatrix}\underline{\underline{1}} & 0\\ 0 & \underline{\underline{a}}\end{pmatrix},$$

where $\underline{\underline{a}}$ is a full matrix with dimension equal to the number of discretized continuum states [25]. In general, the values of the diagonal elements a_{ii} decrease with i and the nondiagonal elements decrease with $|i-i'|$. Multiplying the coefficient vector $\underline{c}$ with this matrix has the result that the coefficients for the true bound states remain unaffected, whereas the coefficients belonging to the continuum states are coupled and damped. The damping is more efficient the farther the wave functions extend into the product channel. In this way, the norm of the wave packet gradually diminishes

when continuum states are populated. Splitting the wave packet is equivalent to introducing an imaginary absorbing potential at large distances [26]. However, the splitting method has the advantage that the part of the wave packet that has been removed can be further propagated on the asymptotic grid, in order to calculate final state distributions.

Since only a limited number of states are included in the basis, this procedure is an approximation. In order to check its general applicability, we performed one-dimensional test calculations (for a one-dimensional model of HCO dissociation) and compared the results from the matrix method with the results obtained from propagating a wave packet on a grid. For a system with only one degree of freedom, one can shift the boundary $R_{\max}$ to very large distances and include states up to high energies, thereby making the approximation better and better. Indeed, perfect agreement between the two approaches was obtained for the dissociation probability. This encouraged us to apply the method also to systems with more than one internal degree of freedom. These exploratory calculations were also used to define an appropriate split function. Of course, the final result, i.e., the dissociation probability, does not depend on the particular form of f_{split}.

The integration of the set of differential equations (3) is straightforward. The method that is mostly used, for time-dependent Hamiltonians, is the so-called split-operator technique [27,28]. However, in the present applications we include up to $N=2000$ wave functions in the basis, which makes these calculations very time consuming too, with the consequence that extensive variations of parameters such as frequency, intensity, and duration of the pulse are prohibited. The reason is that at each time step an $N\times N$ matrix has to be diagonalized in order to apply the time evolution operator. Under certain conditions, which are met in the present calculations, a drastic reduction of the computer time can be achieved by applying a transformation to a new basis.

Let us assume that the molecule-field interaction can be written as

$$\hat{W}(t)=E(t)\hat{\mu}_{\text{eff}}, \tag{6}$$

i.e., that the time-dependent part and the coordinate-dependent parts are separated. In the present applications, this is the case for linear polarization of the electric field. Diagonalizing the corresponding matrix for the dipole operator, $\underline{\underline{\mu}}_{\text{eff}}$, by a matrix $\underline{\underline{T}}$ leads to the new Schrödinger equation

$$i\frac{d}{dt}\tilde{\underline{c}}(t)=[\underline{\underline{T}}^t\underline{\underline{H}}_0\underline{\underline{T}}+E(t)\tilde{\underline{\underline{\mu}}}_{\text{eff}}]\tilde{\underline{c}}(t), \tag{7}$$

where the vector of new coefficients is given by

$$\tilde{\underline{c}}(t)=\underline{\underline{T}}^t\underline{c}(t). \tag{8}$$

Note that after the transformation the new dipole matrix, $\tilde{\underline{\underline{\mu}}}_{\text{eff}}$, is diagonal while $\underline{\underline{T}}^t\underline{\underline{H}}_0\underline{\underline{T}}$ is a full matrix.

The short-time propagator for a time step $t\rightarrow t+\Delta t$, in matrix notation, is then given by

$$\begin{aligned}\exp[-i\underline{\underline{H}}(t)\Delta t]&=\exp\{-i[\underline{\underline{T}}^t\underline{\underline{H}}_0\underline{\underline{T}}+E(t)\tilde{\underline{\underline{\mu}}}_{\text{eff}}]\Delta t\}\\&\approx\exp\left[-iE(t)\tilde{\underline{\underline{\mu}}}_{\text{eff}}\frac{\Delta t}{2}\right][\underline{\underline{T}}^t\exp(-i\underline{\underline{H}}_0\Delta t)\underline{\underline{T}}]\\&\quad\times\exp\left[-iE(t)\tilde{\underline{\underline{\mu}}}_{\text{eff}}\frac{\Delta t}{2}\right].\end{aligned} \tag{9}$$

The advantage of the basis transformation is obvious: Since the matrix

$$\underline{\underline{T}}^t\exp(-i\underline{\underline{H}}_0\Delta t)\underline{\underline{T}}$$

is independent of time, it has to be calculated only once at the beginning of the propagation. In particular, only a single matrix diagonalization is required in the entire calculation. Thus, during the propagation only one matrix-vector multiplication has to be performed for each time step. Application of the other two exponential functions is trivial, because $\tilde{\underline{\underline{\mu}}}_{\text{eff}}$ is a diagonal matrix. The matrix of the split function, $\underline{\underline{f}}$, also has to be transformed, i.e., the vector $\tilde{\underline{c}}$ has to multiplied—from the left—with $\underline{\underline{T}}^t\underline{\underline{f}}\underline{\underline{T}}$ rather than $\underline{\underline{f}}$.

III. CALCULATIONS FOR HCO

A. Potential and dipole moment

In the present paper we apply the theory outlined in the preceding section to the formyl radical, HCO, in its electronic ground state $\tilde{X}^2A'$. The spectroscopy and unimolecular dissociation of this simple triatomic molecule have been amply studied in recent years, both experimentally and theoretically [29], and therefore HCO is a good candidate for investigating excitation and dissociation with strong laser fields. A very accurate *ab initio* potential energy surface (PES) exists, which has been used in several recent dynamics calculations [30,31]. Figure 1 shows contour plots of the PES as a function of R and r for fixed angle γ and as a function of R and γ for fixed r. Here, R, r, and γ are the usual Jacobi coordinates for the fragmentation into H and CO: R is the distance from H to the center of mass of CO, r is the CO vibrational coordinate, and γ is the angle between **R** and **r** with $\gamma=0$ corresponding to linear HCO. These coordinates are used throughout our calculations. Figure 2(a) shows a cut through the PES along the dissociation path. In what follows, energy is normalized so that $E=0$ corresponds to $\text{H}+\text{CO}(r_e)$. With this normalization the threshold for dissociation is at $E=0.134$ eV.

The characteristic features of HCO can be summarized as follows. (i) The PES has a shallow well of 0.834 eV with respect to $\text{H}+\text{CO}(r_e)$ and a small barrier separates the well region from the product channel. (ii) Because of the small well depth there are only 15 bound states, a number that is extremely small for a triatomic molecule. (iii) The CO degree of freedom is very weakly coupled to the other two modes, especially the dissociation coordinate R. (iv) As a consequence of this weak coupling there exists a long progression of resonances, i.e., quasibound states embedded into the continuum, with relatively long lifetimes up to very high energies above the threshold. The dynamics calculations of Keller *et al.* [30,31] reproduce the measured energy levels and resonance widths for both HCO [32] and DCO [33] very

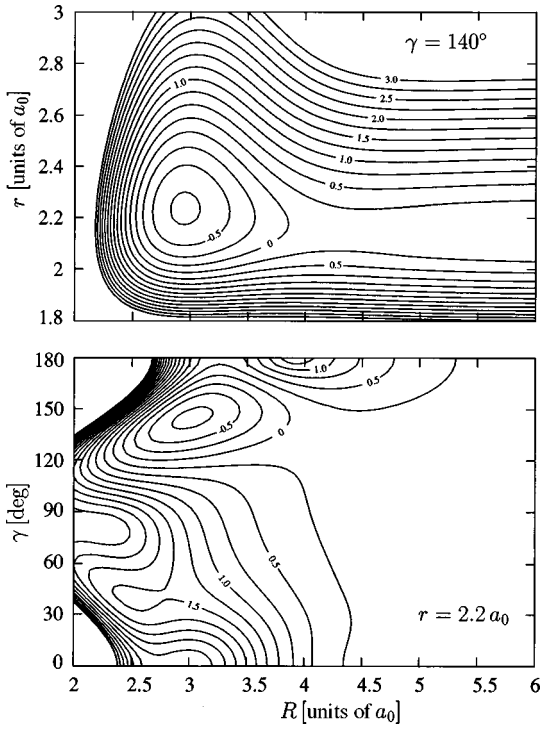

FIG. 1. Two-dimensional contour plots of the HCO potential energy surface for fixed angle $\gamma=140°$ (upper panel) and fixed CO distance $r=2.20a_0$ (lower panel). The highest contour is 3 eV with respect to the H+CO (r_e) asymptote and the spacing is 0.25 eV.

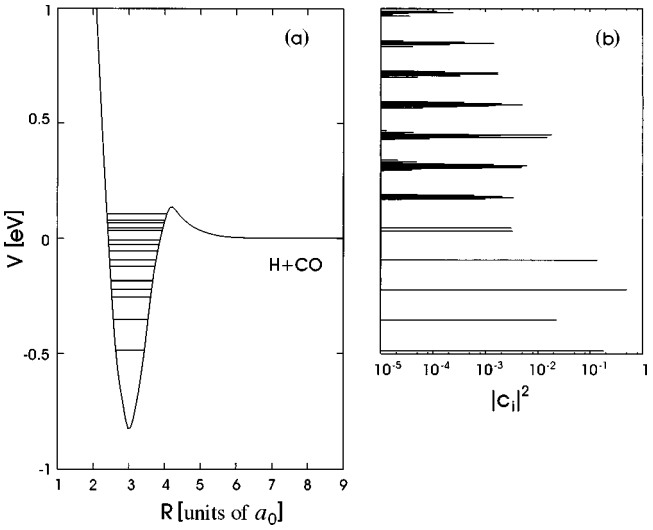

FIG. 2. (a) Cut along the minimum energy path of the HCO potential energy surface as a function of the dissociation coordinate R; r and γ are optimized for each value of R. The horizontal lines indicate the energies of the 15 bound states. (b) Probabilities $|c_i|^2$ with which the bound and the continuum states are populated at the end of the pulse. The parameters of the field are the same as in Fig. 9.

well over a large range of energies, which underlines the high accuracy of the calculated PES.

In addition to the PES, one also needs the dipole moment function $\vec{\mu}$ and its dependence on the coordinates. Like the PES, $\vec{\mu}$ has been calculated by an *ab initio* method using the MOLPRO program package [34]. It lies in the molecular plane and has two components, $\vec{\mu}=(\mu_x,0,\mu_z)$. The z axis is chosen to be parallel to the CO bond and the x axis is perpendicular to it; the y axis is chosen to be perpendicular to the molecular plane. The present calculations have the character of ''realistic model calculations'' and therefore it was not our goal to employ a most accurate dipole moment function in the dynamics calculations. For this reason we calculated the dipole moments μ_x and μ_z for a limited number of coordinate points only and fitted them to simple analytical expressions according to

$$\begin{aligned}\mu_x(R_{\mathrm{HC}},R_{\mathrm{CO}},\alpha)=&-0.012\,263\,906\,958\,558\,87+1.391\,453\,253\,479\,689\exp(-1.2R_{\mathrm{HC}})+0.071\,563\,961\,513\,985\,04\\&\times\exp[-(\alpha-100)^2/1000]-0.089\,676\,589\,964\,959\,2\exp[-(\alpha-60)^2/100]\\&-0.061\,899\,700\,726\,940\,98\arctan[10.0(R_{\mathrm{HC}}-3)]+0.398\,432\,144\,156\,406\,8\arctan[0.5(R_{\mathrm{CO}}-2.1)],\end{aligned}\tag{10}$$

$$\begin{aligned}\mu_z(R_{\mathrm{HC}},R_{\mathrm{CC}},\alpha)=&-0.616\,498\,481\,764\,975\,5+1.038\,715\,052\,345\,678\exp(3/5-\alpha/100)\\&+0.121\,834\,867\,711\,874\,4\arctan[2(R_{\mathrm{HC}}-3)]+0.762\,275\,202\,366\,669\,5\arctan(R_{\mathrm{CO}}-2)\\&+0.169\,491\,196\,659\,661\,4\arctan(\alpha/50-2).\end{aligned}\tag{11}$$

R_{HC} and R_{CO} are the HC and CO bond distances (in units of a_0) and α is the HCO bond angle (in degrees). The dipole moments are given in atomic units.

B. Numerical details

Using Jacobi coordinates R, r, and γ and the transformation $\psi(R,r,\gamma)=\tilde{\psi}(R,r,\gamma)/(Rr)$ for the wave function, the Hamilton operator for the free HCO molecule reads (the total angular momentum quantum number is $J=0$)

$$\hat{H}_0=\hat{T}(R,r)+B(R,r)\hat{j}^2+V(R,r,\gamma),\tag{12}$$

where

$$\hat{T}(R,r)=-\frac{1}{2m}\frac{\partial^2}{\partial R_2}-\frac{1}{2\mu}\frac{\partial^2}{\partial r_2}\tag{13}$$

is the kinetic energy operator for the motion in R and r, $B(R,r)=1/(2mR^2)+1/(2\mu r^2)$ is the coordinate-dependent rotational constant of the CO moiety, $\hat{j}$ is the rotational angular momentum operator of CO, and $V(R,r,\gamma)$ is the potential energy surface. m and μ are the reduced masses for H-CO and CO, respectively.

The calculation of the bound state energies and corresponding wave functions proceeds in the same way as described in Ref. [35]. In short, first we define primitive bases in R, r, and γ. Subsequently, the resulting 3D basis is internally contracted to yield a more appropriate basis and then this new basis is truncated, that is, only states with energies below a certain value are included. Diagonalization of the Hamiltonian in this contracted-truncated basis gives both the energies and the wave functions. The primitive bases in the two stretch coordinates are series of equally spaced grid points (Fourier discrete variable representation, DVR); the grids range from $R_{\min}=1.8144a_0$ to $R_{\max}=9a_0$ with $N_R=44$ and from $r_{\min}=1.8678a_0$ to $r_{\min}=3.2a_0$ with $N_r=22$. The primitive basis functions in the angular coordinate are Legendre polynomials, i.e., the eigenfunctions of $\hat{j}^2$; the number of polynomials included is $N_\gamma=76$. The cutoff energy is chosen to be 1.75 eV resulting in a total basis of dimension $N_{\text{tot}}=8987$.

The large value for $R_{\max}$ guarantees that most of the bound-state wave functions in the box have the qualitative character of continuum wave functions despite the fact that they are finite and do not extend to infinity. The main computer time is spent before the propagation for diagonalizing the Hamiltonian and for calculating the matrices $\underline{\underline{\mu}}_{\text{eff}}$ and $\underline{\underline{f}}$ needed in the propagation of the wave packets in the state space.

In order to test the matrix method, we performed also a few calculations in which the wave packet is propagated on the 3D grid in coordinate space. The time propagation is done using the split-operator technique [27,28], i.e., the short-time evolution operator is approximated by

$$\begin{aligned}\exp[-i(\hat{T}+B\hat{j}^2+V+\hat{W})\Delta t] &\approx \exp\left(-i\hat{T}\,\frac{\Delta t}{2}\right)\exp[-i(V+B\hat{j}^2+\hat{W})\Delta t] \\ &\quad\times\exp\left(-i\hat{T}\,\frac{\Delta t}{2}\right),\end{aligned} \tag{14}$$

where $\hat{T}+B\hat{j}^2$, V, and $\hat{W}(t)$ are the kinetic energy operator, the potential energy, and the coupling operator, respectively. Similar to the calculation of the bound states, the kinetic energy operators in R and r are evaluated by fast-Fourier transform [13]. The angular degree of freedom is treated by expanding the wave packet in terms of the eigenfunctions of $\hat{j}^2$, that is, the Legendre polynomials $P_j(\gamma)$. In order to avoid the calculation of large time-dependent matrices for many grid points (R,r), one can make a transformation to a new basis, in which the operator for the angle γ is diagonal (Gauss-Legendre DVR) [36,37]. The matrix for the operator $\hat{j}^2$, which was diagonal in the original basis, now becomes nondiagonal. The corresponding propagator becomes a four-dimensional data structure indexed by R, r, j, and j'. In each time step, two fast-Fourier transforms of the three-dimensional wave packet and a multiplication of the four-dimensional angular momentum propagator with the wave packet is necessary, which makes the propagation very expensive.

Note that the transformation used in the matrix propagation and the angular-DVR transformation in the grid propagation are completely different. The grid propagation method uses exactly the same grid parameters as in the calculation of the stationary wave functions in the box.

In addition to the two types of quantum-mechanical calculations, we also performed classical mechanics calculations for comparison. The exact quantal approaches are exceedingly time consuming and therefore only applicable for the smallest systems. The classical calculations are much less demanding and therefore they can be used for studying bigger systems (provided the potential is available). This requires, however, that one assesses their accuracy by comparison with exact calculations. The trajectory calculations require three steps [3]. (i) The definition of the initial conditions for the three coordinates R, r, and γ and for their conjugate momenta P_R, P_r, and P_γ, respectively. In the present work the initial values are randomly selected from normal distributions, which resemble the quantum-mechanical distributions in coordinate space and momentum space, respectively (see, for example, Chap. 5 in Ref. [3]). Only those points in the six-dimensional phase space are accepted, which roughly match the zero-point energy of the ground vibrational state. (ii) Integration of Hamilton's equations of motion; in the present work this is done by a Runge-Kutta algorithm. (iii) Monte Carlo averaging over many trajectories; typically, 3000 trajectories are run for each pulse.

In the present work we assume that the electric field is polarized along the body-fixed z axis of HCO, i.e., $W=E_z(t)\mu_z(R,r,\gamma)$. Except where otherwise stated, we use an envelope for the electric field pulse that grows like $\sin^2$ within 605 fs, reaches a plateau of length 2420 fs, and finally decreases again like $\sin^2$:

$$E(t)=\begin{cases}\sin^2\left(\dfrac{t\pi}{1210\text{ fs}}\right)\sin(\omega t) & \text{for} \quad 0\leqslant t<605\text{ fs},\\ \sin(\omega t) & \text{for} \quad 605\text{ fs}\leqslant t<3025\text{ fs},\\ \sin^2\left(\dfrac{t\pi}{1210\text{ fs}}\right)\sin(\omega t) & \text{for} \quad 3025\text{ fs}\leqslant t<3630\text{ fs}.\end{cases} \tag{15}$$

For comparison, a few calculations are also performed with a pure $\sin^2$ function with a peak at 302.5 fs and without a plateau, i.e.,

$$E(t)=\sin^2\left(\frac{t\pi}{605\ \text{fs}}\right)\sin(\omega t). \tag{16}$$

IV. RESULTS

In order to understand the subsequent discussion, we depict in Fig. 3 the vibrational energy spectrum of HCO and the corresponding assignment. v_1 and v_2 are the HC and the CO stretching quantum numbers basically related to motion in R and r, respectively, and v_3 is the bending quantum number. We first discuss the general accuracy of the matrix propagation method and then show examples for excitation of the molecule with different frequencies, intensities, and pulse lengths.

A. Convergence tests

There are basically two parameters that are important for the accuracy of the matrix propagation method, the density of states with which the continuum is approximated and the number of states included in the expansion of the wave packet. The density is determined by the size of the box, that is, $R_{\max}$. The total number of states is essentially dictated by the computer time required for calculating the states, their wave functions, and the various matrices. In the present applications the lowest 2000 energy levels have been determined and this number represents the maximum of states that can be included.

The general applicability of the method to describe dissociation of HCO into H and CO and the density of states in particular has been tested in the following way. We assume that HCO is initially excited to a particular resonance state i, i.e., a quasibound state whose wave function is localized in the region of the potential well and exponentially decays towards the boundary of the box. The initial coefficients are such that $c_i(0)=1$ for this single state and zero otherwise. If we then propagate the system of linear equations, ignoring the external field ($\hat{W}=0$), probability is slowly transferred to other nearby states. This coupling is introduced through the cutoff function $f_{\text{split}}(R)$ as described above. Without the cutoff function, the norm of the initial state would remain constant, because all states in the basis—by construction—are orthogonal to each other. Multiplying the wave functions with $f_{\text{split}}(R)$ destroys the orthogonality and thus flow of probability from the initial state to other states becomes possible. Plotting the logarithm of the norm of the wave packet as a function of time yields—after some ''induction'' period—a perfectly straight line. The rate of dissociation extracted from the slope of this line was found to be in very good agreement with the rate obtained from the Lorentzian resonance widths in the time-independent calculations in Ref. [30]. This check has been performed for several resonance states. The largest deviation found was of the order of 25% and very likely can be attributed to the quite different grid sizes used in the two calculations (the grid in the time-independent calculations of Ref. [30] was denser and therefore more appropriate for the purely spectroscopic purposes).

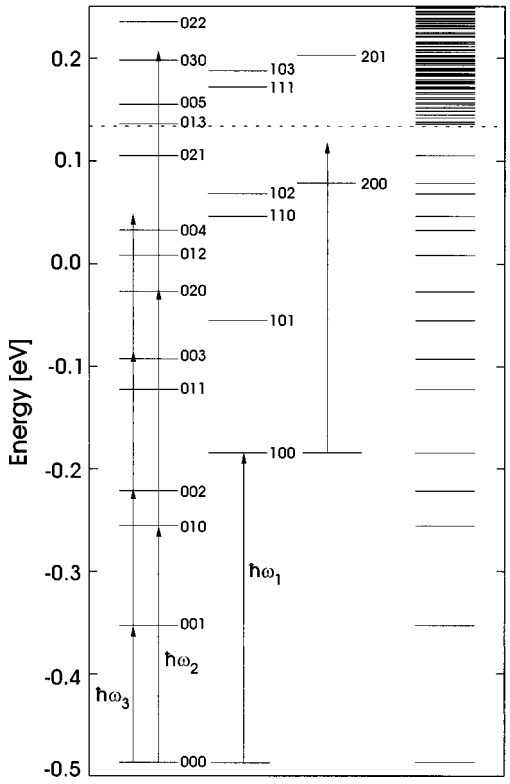

FIG. 3. Energy spectrum of HCO with assignment (v_1,v_2,v_3), where v_1, v_2, and v_3 are the number of quanta in the HC stretching mode, the CO stretching mode, and the bending mode, respectively. The outermost column on the right-hand side contains all states irrespective of the assignment. The broken horizontal line marks the dissociation threshold. The assigned levels above the threshold represent resonance states as calculated in Ref. [30]. The vertical arrows illustrate the multiphoton excitation as described in the text.

If the density of ''continuum'' states was not sufficiently large, the dissociation would yield dissociation rates in disagreement with the time-independent calculations.

Once the discretized continuum states are fixed, the main convergence parameter is the number of states and thus the highest state included in the expansion of the wave packet. When the external field excites the molecule, higher and higher vibrational levels become populated, i.e., the expectation value of the molecular Hamiltonian on average steadily increases. Once states in the continuum are excited, the molecule begins to dissociate. If the states close to the high-energy limit of the basis become excited, artificial effects caused by the finite number of expansion functions are expected and the results cannot be trusted any longer. This scenario is believed to happen with very intense electric fields.

In order to test the convergence with respect to the number of states, we performed several calculations with relatively strong fields. Since the grid calculations are extremely time consuming, the short laser pulse of Eq. (16) is used in these calculations. The central frequency equals the fundamental frequency of the bending mode (see Fig. 3). In Fig. 4(a) we show the norm of the wave packet calculated within the box, $N(t)=\langle\Phi(t)|\Phi(t)\rangle$, for two different intensities. The dissociation probability is given by $P(t)=1-N(t)$. For the smaller intensity of $10^{13.7}$ W/cm^2 the excitation is modest and only $\sim$55% of the wave packet dissociates. In this case

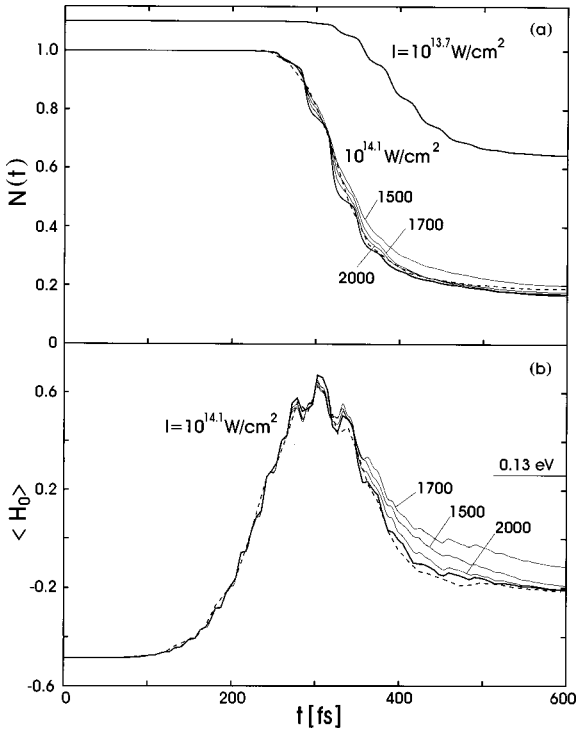

FIG. 4. (a) The norm of the wave packet, $N(t)$, for two intensities. $I=10^{13.7}$ W/cm^2: the results of the grid propagation (thick solid line) and of the matrix propagation with 2000 basis functions are almost indistinguishable; for clarity of the figure the two curves are shifted upward by a value 0.1. $I=10^{14.1}$ W/cm^2: comparison of the grid propagation (thick solid line), three different matrix propagations with 1500, 1700, and 2000 basis functions (thin curves), and the classical trajectory calculation (dashed curve). The short pulse of Eq. (15) is used and the frequency is the fundamental frequency of the bending mode, ω_3. (b) The expectation value of the molecular Hamiltonian. All other details are the same as in (a).

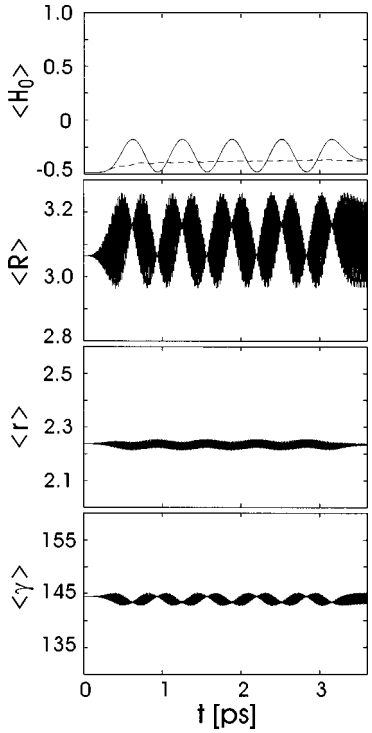

FIG. 5. Expectation values of the molecular Hamiltonian H_0 (in eV) and the three internal coordinates R, r (in a_0), and γ (in degrees) as functions of time. The dashed curve is the average energy as obtained from the trajectory calculation. The long pulse defined in Eq. (15) is used with $\omega=0.302$ eV corresponding to the first excitation in the ν_1 mode (ω_1); the intensity is 10^{13} W/cm^2.

the matrix calculation with the maximum of 2000 levels agrees perfectly with the grid propagation. The small undulations superimposed on $N(t)$ reflect the oscillations of the field. When the intensity is increased by a factor of about 2.5, the dissociation probability increases to about 80%. In this case the agreement between the grid calculation and the calculation with 2000 states is good, but not perfect; small deviations occur early on. However, comparing calculations with 1500, 1700, and 2000 states included in the basis shows a systematic convergence towards the result obtained with the grid propagation, which is assumed to be numerically exact. A basis size with presumably 2500 states is expected to yield good agreement with the exact grid calculation. The dissociation probability obtained from the classical calculations is in very good accord with the quantum results.

Figure 4(b) shows for the higher intensity the expectation value of the molecular Hamiltonian, $\langle H_0\rangle$, as a function of time. The external field excites the molecule very rapidly from the ground-state level to an energy high above the dissociation energy. When the pulse reaches its maximum around 300 fs, $\langle H_0\rangle$ also comes to a maximum. Beyond this maximum the excitation through the external field begins to decrease. Since at the same time the states above threshold dissociate, more and more of the high-energy states are removed from the wave packet, which has the net effect that the molecular energy decreases below the threshold energy. When the pulse is switched off at 605 fs and when all continuum states are dissociated, $\langle H_0\rangle$ becomes constant again. The maximum of about 0.7 eV is not too far away from the energy of the highest state in the basis (1.2 eV) and thus it is not surprising that the result obtained with the $N=2000$ basis does not perfectly agree with the grid propagation. The calculations with the reduced basis sizes agree even less well with the exact calculation. Again, the result of the classical approach is in surprisingly good agreement with the quantum-mechanical propagations for the entire duration of the pulse.

B. Mode-specific ladder climbing

In this section we compare the multiphoton excitation and dissociation caused by excitation in the three fundamental modes, i.e., the central frequency of the pulse is equal to the fundamental energy spacing in each mode (see Fig. 3). The long pulse of Eq. (15) is used and the intensity is 10^{13} W/cm^2 in all cases. Figure 5 shows the results for the H-CO stretching mode. The three lower panels depict the expectation values of the Jacobi coordinates. $\langle R\rangle$ shows a pronounced oscillatory motion, whereas $\langle r\rangle$ and $\langle\gamma\rangle$ remain almost constant except for some small undulations. This means that, as expected, essentially the laser excites motion along R, or expressed differently, only states of the type $(v_1,0,0)$ are populated. The expectation value of the energy of the molecule, $\langle H_0\rangle$, shown in the upper part of Fig. 5, has a perfect sinusoidal behavior, but on the average remains quite small. This

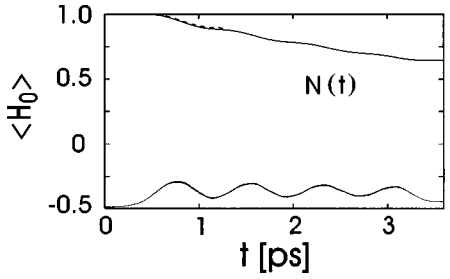

FIG. 6. The expectation value of the molecular Hamiltonian H_0 (in eV) and the norm of the wave packet $N(t)$ as functions of time. The frequency of the pulse is $\omega = 0.286$ eV roughly corresponding to half of the (0,0,0)-(2,0,0) transition energy. The intensity is $10^{13.5}$ W/cm^2. The dashed curve is the result from a (short) grid calculation in order to test the accuracy of the matrix propagation.

behavior is reminiscent of Rabi oscillations in a two-level system driven by an external field [2]. Here, the states that are involved are the ground vibrational state and the first excited state of the ν_1 mode, (1,0,0). The minima and maxima of $\langle H_0 \rangle$ agree well with the energies of these two states. Without showing further results, we note that the period of the oscillations decreases with increasing intensity. The very fast oscillations superimposed on the expectation values reflect the oscillations of the external force with which the molecule is driven. They do not change with the field intensity.

Because of the large anharmonicity in the ν_1 mode, the next ''staircase,'' (2,0,0) is significantly out of resonance, and therefore its excitation is exceedingly small (see Fig. 3). Thus, as the pulse is driving the molecule, probability is reshuffled between the two states (0,0,0) and (1,0,0), despite the fact that many more states are present. As a consequence, the norm of the wave packet, $N(t)$, remains almost unity for the entire period, i.e., the dissociation probability is negligibly small. The ladder climbing stops at the first step and therefore the molecule can never reach the continuum and dissociate, although it is directly excited in the dissociation mode. The ladder climbing can be made more efficient, for example, by detuning the excitation frequency. If ω is adjusted so that 2ω approximately corresponds to the (0,0,0)-(2,0,0) transition, the continuum can be reached more efficiently and the dissociation probability is significantly enhanced. Figure 6 shows an example for an intensity of $10^{13.5}$ W/cm^2; the same calculation for the fundamental excitation frequency ω_1 yields a dissociation probability that is almost zero. Also shown in this figure, for comparison, is the result from a (short) grid propagation.

The classical result for the mean energy does not reproduce the oscillations of $\langle H_0 \rangle$ in Fig. 5. This is what one would expect, especially since only two quantum states are significantly populated. However, the average is well reproduced. The classical dissociation probability is also almost zero, just like its quantum-mechanical counterpart.

Figure 7 shows the same quantities as in Fig. 5 but for excitation with the fundamental in the ν_2 mode. As expected, the molecule is now excited along the CO bond r as indicated by the large oscillations of $\langle r \rangle$. HCO has a surprisingly long progression of pure states $(0,v_2,0)$, in the bound part of the potential as well as in the continuum [30]. Since this progression is remarkably harmonic (see Fig. 3), the laser

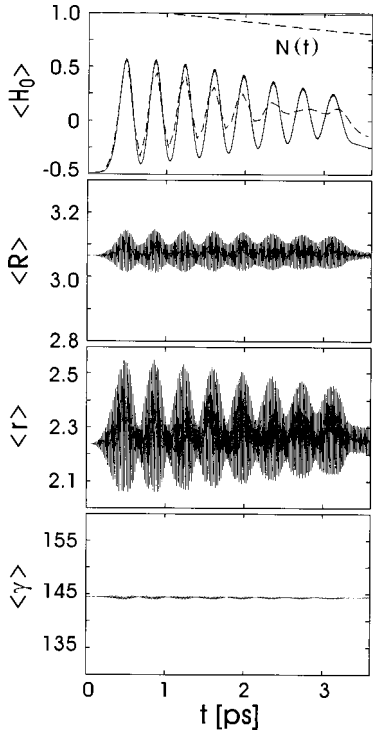

FIG. 7. Expectation values of the molecular Hamiltonian H_0 (in eV) and the three internal coordinates R, r (in a_0), and γ (in degrees) as functions of time. The upper panel also contains the norm of the quantum-mechanical wave packet inside the ''box,'' $N(t)$. The two dashed curves are the corresponding data obtained from the trajectory calculation. The long pulse defined in Eq. (15) is used with $\omega = 0.231$ eV corresponding to the first excitation in the ν_2 mode (ω_2); the intensity is 10^{13} W/cm^2.

can efficiently drive the molecule up this ''staircase.'' This is manifested by the large amplitude of the expectation value of the molecular Hamiltonian, which oscillates in a quite regular manner between the maxima and minima. Although the pulse is exactly the same as in Fig. 5, the energy transfer from the field to the molecule is much larger. However, the dissociation probability is again extremely small, despite the effectiveness of the excitation process. The reason is that the motion in r is only weakly coupled to the dissociation coordinate R, which is manifested by the small amplitude of $\langle R \rangle$. In other words, the dissociation rates for the pure CO stretching resonances are very small [30]. Thus, the laser strongly excites the molecule in the r direction, but this does not lead to noticeable dissociation, at least not on the time scale of a few picoseconds.

In contrast to the results in Fig. 5, the classical calculations reproduce the strong oscillations of $\langle H_0 \rangle$ remarkably well, at least for the first part of the pulse. Because several states $(0,v_2,0)$ are excited, the wave function $\Phi(t)$ has the behavior of a localized wave packet, which bounces back and forth between the inner and the outer turning point. Apparently, this classical-like behavior is well reproduced by the classical calculations. As time elapses, the ''coherence'' is gradually destroyed with the consequence that the oscillations are damped. The classical calculations give rise to a dissociation probability that is significantly larger than in the quantum calculations. The deviation becomes significant after about 1 ps; we suspect it is the ''dephasing'' of the ''clas-

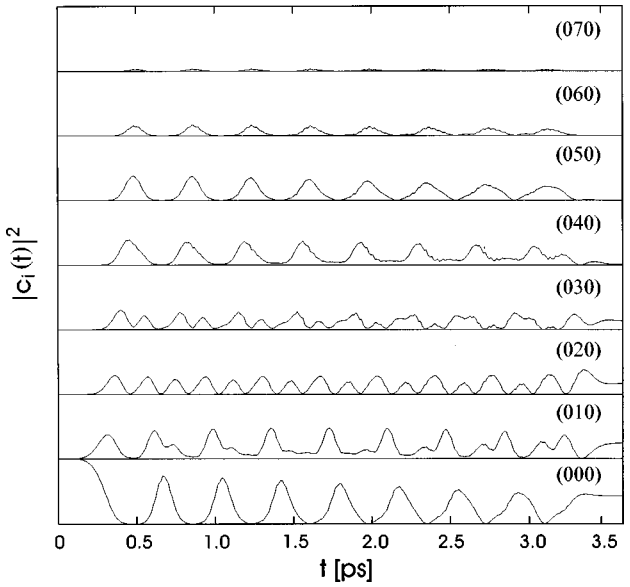

FIG. 8. Time dependence of the populations $|c_i(t)|^2$ for the pure CO stretching bound and resonance states $(0,v_2,0)$. The parameters are the same as in Fig. 7.

sical wave packet'' that causes the failure of the classical calculation.

The ladder climbing is additionally illustrated in Fig. 8, where we show the probabilities $|c_i(t)|^2$ of the pure CO stretching states $(0,v_2,0)$ as functions of time. All probabilities show a pronounced oscillatory structure, which is similar to the oscillatory structures in Fig. 7. Details of these oscillations, however, depend strongly on the particular level. When the laser begins to act on the molecule, it drives the quantum system rapidly up the ladder of pure CO stretching states. The excitation follows basically a sequential steplike mechanism, i.e., the molecule climbs from (0,0,0) to (0,1,0), from (0,1,0) to (0,2,0), etc. The oscillations with a period of about 0.6 ps are again the Rabi-like oscillations mentioned already in Fig. 5. However, while in the latter case only two states were involved, here several states are embraced. We note again that the period becomes smaller with increasing intensity of the field, as predicted by the simple two-state model [38].

Finally, we show in Fig. 9 results for excitation in the bending mode ν_3. This ladder is also quite harmonic and therefore can be climbed easily. In contrast to the ν_2 mode, however, the bending motion is more strongly coupled to the dissociation mode—manifested by the relatively large expectation value of $\langle R\rangle$—with the result that breaking apart into H and CO is much more probable. The mean molecular energy is significantly smaller than when the r mode is excited; nevertheless, the dissociation probability is considerably larger. In this case we also performed a calculation on the grid. The two dissociation probabilities and expectation values of $\hat{H}_0$ agree perfectly. In view of the convergence tests in Fig. 4, this agreement is expected, because the degree of excitation, reflected by the maxima of $\langle H_0\rangle$, at all instants is well below the highest state in the basis. The classical calculations reproduce the average of $\langle H_0\rangle$ quite well but again significantly overestimate the dissociation probability. As in

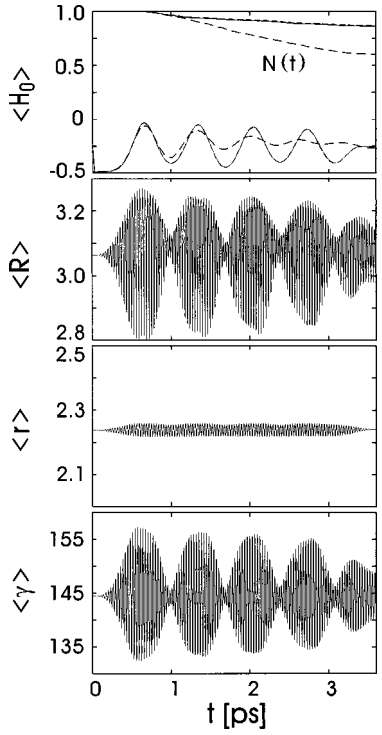

FIG. 9. Expectation values of the molecular Hamiltonian H_0 (in eV) and the three internal coordinates R, r (in a_0), and γ (in degrees) as functions of time. The upper panel also contains the norm of the quantum-mechanical wave packet inside the ''box,'' $N(t)$; the solid line results from the grid propagation and the line with the short dashes is the result of the matrix propagation. The two curves with the long dashes are the corresponding data obtained from the trajectory calculations. The long pulse defined in Eq. (15) is used with $\omega=0.134$ eV corresponding to the first excitation in the ν_3 mode (ω_3); the intensity is 10^{13} W/cm^2.

Fig. 7, the deviations become significant after about 1 ps, when the dephasing of the classical calculation sets in.

C. Distributions at the end of the pulse

The matrix propagation method also allows us to analyze the distribution of states (including both the true bound states and the states in the continuum) at the end of the pulse, i.e., which states are populated and which are only marginally excited. This is achieved in the following way. After each time step the coefficient vector $\underline{c}$ is multiplied with the matrix $\underline{\underline{f}}$ in order to mimic the dissociation. The vector $\Delta\underline{c} \equiv(\underline{\underline{1}}-\underline{\underline{f}})\underline{c}$ is thereby removed from the wave packet. As the calculation continues, each component of Δc is separately propagated by the time evolution operator $\exp(-iE_it)$. At the end of the pulse, the part of $\underline{c}$, which has not yet been removed, and all $\Delta\underline{c}$ are coherently summed.

In Fig. 2(b) we show one example of such a ''final state distribution''; the corresponding time-dependent picture is given in Fig. 9 (excitation with the bending frequency ω_3). Since in this case the dissociation is comparatively small, mainly the bound states are populated with state (0,0,2) having the maximum probability. Nevertheless, the continuum states are clearly populated however small their probabilities are. The resonant ladder climbing, which started in the bound manifold, clearly persists into the continuum. Although the

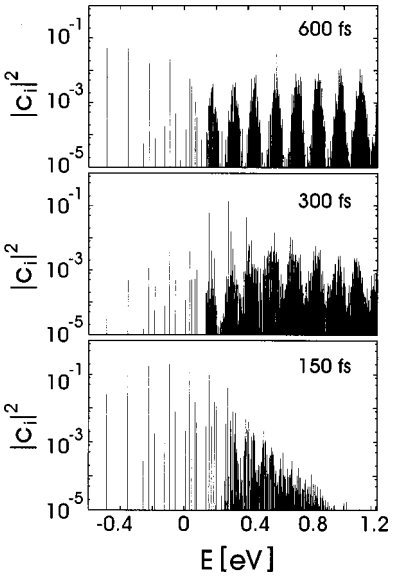

FIG. 10. Probabilities $|c_i|^2$ with which the bound and continuum states are populated at the end of the propagation for three different pulse durations. The pulses have the form as given in Eq. (16) and the intensity is $10^{14.1}$ W/cm^2.

density of quasicontinuum states is very high (right-hand column in Fig. 3), only relatively few of them are populated as manifested by the deep minima between the different clumps separated by $\hbar\omega_3$. The fact that the molecule absorbs more photons than required for breaking the bond is called *above threshold dissociation* and has been observed in several theoretical studies of diatomic molecules [39].

With decreasing pulse duration, the resonance condition becomes less and less fulfilled with the consequence that the clumps become gradually broader and smeared out. The influence of the pulse length on the clump structure of the final state distribution is illustrated in Fig. 10. Shown are the final values of the probabilities $|c_i|^2$ for three different pulses having envelopes as defined in Eq. (16) with pulse lengths of 600, 300, and 150 fs, respectively. The shorter the pulse, the less well fulfilled is the resonance condition and the more blurred is the clump structure. While for the longest two pulses states up to the energetic cutoff are populated, for the 150 fs, pulse the population rapidly diminishes towards the highest state in the basis.

V. SUMMARY AND OUTLOOK

We have described a practicable method for studying vibrational excitation with subsequent dissociation of molecules driven by an—in principle—arbitrary external electric field. The cornerstone of the method is the expansion of the wave function in terms of *all* bound-state wave functions of the free molecule and a large set of discretized continuum states. The latter are bound states defined in a box, which is so large that the wave functions have the character of continuum-state wave functions. Provided the coupling operator factorizes into a time-dependent part, which is independent of the coordinates, and a coordinate-dependent term, which does not depend on time, an efficient algorithm for the propagation can be applied, which requires only one matrix-vector multiplication per time step.

We have applied the method to the multiphoton excitation and dissociation of HCO in its ground electronic state. Comparisons to numerically exact calculations on a three-dimensional grid have shown that, first, the state-expansion method is considerably faster than the traditional grid propagation and, second, it is very accurate provided the degree of excitation is not too large. The main convergence parameter is the number of states included in the basis. If the molecule climbs up the ladder of vibrational states too quickly, states at the upper end of the ladder become significantly populated and spurious effects can occur. Thus, the expansion method is the method of choice for small or medium coupling strengths.

We also tested the accuracy of the classical trajectory method. The agreement with the results of the exact grid propagation is very good for short but intense pulses. This holds true both for the average molecular energy and the dissociation probability. The agreement is less good for the weaker but longer pulses. Thus, the classical calculations are trustworthy only when the interaction time is short, below 1 ps or so in the present case.

The internal dynamics of HCO is mainly regular and this is reflected by the quite regular behavior of the expectation values of the coordinates and the average molecular energy; they show clear-cut Rabi-type oscillations over the entire duration of the pulse. The regular dynamics is also manifested by the pronounced mode specificity of the ladder climbing and the dissociation probability. For example, excitation with the fundamental of the CO stretching mode does not lead to noticeable dissociation. In contrast, excitation with the fundamental frequency in the bending mode does result in a significant bond rupture, although the bending frequency is roughly half of the CO frequency, that is, more photons are required to break the bond. In a second publication we will present results for HNO. The HNO potential well is roughly three times deeper than the HCO well with the result that there are many more bound states and a considerably higher density of states. As a consequence, the dynamics is more irregular and that is clearly shown by the dissociation probability.

ACKNOWLEDGMENTS

The authors gratefully acknowledge financial support from the Deutsche Forschungsgemeinschaft within the Schwerpunktsprogramm ''Zeitabhängige Phänomene und Methoden in Quantensystemen in der Physik und Chemie.''

[1] *Femtosecond Chemistry*, edited by J. Manz and L. Wöste (Verlag Chemie, Weinheim, 1995).

[2] R. Loudon, *The Quantum Theory of Light* (Oxford University Press, Oxford, 1983).

[3] R. Schinke, *Photodissociation Dynamics* (Cambridge University Press, Cambridge, 1993).

[4] S. Mukamel, Annu. Rev. Phys. Chem. **41**, 647 (1990).

[5] W. Domcke and G. Stock, Adv. Chem. Phys. **100**, 1 (1997).

[6] V. N. Bagratashvili, V. S. Letokhov, A. A. Makarov, and E. A. Ryabov, *Multi Photon Infrared Laser Photophysics and Photochemistry* (Harwood, London, 1985).
[7] D. W. Lupo and M. Quack, Chem. Rev. **87**, 181 (1987).
[8] M. Quack, Infrared Phys. **29**, 441 (1989).
[9] M. Quack, Infrared Phys. Technol. **36**, 365 (1995).
[10] T. Elsaesser and M. C. Nuss, Opt. Lett. **16**, 411 (1991).
[11] C. Ludwig, W. Frey, M. Woerner, and T. Elsaesser, Opt. Commun. **102**, 447 (1993).
[12] D. J. Maas, D. I. Duncan, A. F. G. van der Meer, W. J. van der Zande, and L. D. Noordam, Chem. Phys. Lett. **270**, 45 (1997).
[13] R. B. Gerber, R. Kosloff, and M. Berman, Comput. Phys. Rep. **5**, 59 (1986).
[14] P. Schwendner, F. Seyl, and R. Schinke, Chem. Phys. **217**, 233 (1997).
[15] Chem. Phys. **217**, 119ff (1997), thematic issue on dynamics of driven quantum systems.
[16] J. Manz, in *Femtochemistry and Femtobiology*, edited by V. Sundström (World Scientific, Singapore, 1997).
[17] W. Gabriel and P. Rosmus, J. Phys. Chem. **97**, 12 644 (1993).
[18] W. Jakubetz and B. L. Lan, Chem. Phys. **217**, 375 (1997).
[19] R. S. Berry, V. Bonačić-Koutecký, J. Gaus, Th. Leisner, J. Manz, B. Reischl-Lenz, H. Ruppe, S. Rutz, E. Schreiber, S. Vajda, R. de Vivie–Riedle, S. Wolf, and L. Wöste, Adv. Chem. Phys. **101**, 101 (1997).
[20] M. Kaluža and J. T. Muckerman, J. Chem. Phys. **105**, 535 (1996).
[21] A. Beil, D. Luckhaus, M. Quack, and J. Stohner, Ber. Bunsenges. Phys. Chem. **101**, 311 (1997).
[22] The numerical treatment is significantly simpler if the molecule cannot dissociate. Then, one can expand the wave function in a set of suitable square-integrable basis functions and derive a set of first-order differential equations. If the basis functions are simple and if the potential energy surface has a simple coordinate dependence, several modes of a polyatomic molecule can be treated (see, for example, Ref. [5] and references therein).
[23] A. J. Dobbyn, M. Stumpf, H.-M. Keller, and R. Schinke, J. Chem. Phys. **104**, 8357 (1996).
[24] R. Heather and H. Metiu, J. Chem. Phys. **86**, 5009 (1987).
[25] Since the bound-state wave functions exponentially decay into the classically forbidden region, they are never really zero except at the boundary of the grid. As a consequence, the unit matrix in $\underline{\underline{f}}$ has a tiny distortion and also the nondiagonal elements are not exactly zero. However, these deviations from the ideal are negligibly small.
[26] G. Jolicard and E. J. Austin, Chem. Phys. **103**, 295 (1986).
[27] J. A. Fleck, J. R. Morris, and M. D. Feit, Appl. Phys. **10**, 129 (1976).
[28] M. D. Feit, J. A. Fleck, and A. Steiger, J. Comput. Phys. **47**, 412 (1982).
[29] D. W. Neyer and P. L. Houston, in *The Chemical Dynamics and Kinetics of Small Radicals*, edited by K. Liu and A. Wagner (World Scientific, Singapore, 1994).
[30] H.-M. Keller, H. Flöthmann, A. J. Dobbyn, R. Schinke, H.-J. Werner, C. Bauer, and P. Rosmus, J. Chem. Phys. **105**, 4983 (1996).
[31] H.-M. Keller, T. Schröder, M. Stumpf, C. Stöck, F. Temps, R. Schinke, H.-J. Werner, C. Bauer, and P. Rosmus, J. Chem. Phys. **106**, 5359 (1997).
[32] J. D. Tobiason, J. R. Dunlop, and E. A. Rohlfing, J. Chem. Phys. **103**, 1448 (1995).
[33] C. Stöck, X. Li, H.-M. Keller, R. Schinke, and F. Temps, J. Chem. Phys. **106**, 5333 (1997).
[34] MOLPRO is a package of *ab initio* programs written by H.-J. Werner and P. J. Knowles, with contributions from J. Almlöf, R. D. Amos, M. J. O. Deegan, S. T. Elbert, C. Hampel, W. Meyer, K. Peterson, R. Pitzer, A. J. Stone, and P. R. Taylor.
[35] A. J. Dobbyn, M. Stumpf, H.-M. Keller, and R. Schinke, J. Chem. Phys. **103**, 9947 (1995).
[36] Z. Bačić and J. C. Light, Annu. Rev. Phys. Chem. **40**, 469 (1989).
[37] A. Untch, K. Weide, and R. Schinke, J. Chem. Phys. **95**, 6496 (1991).
[38] C. Cohen-Tannoudji, B. Diu, and F. Laloë, *Quantum Mechanics* (Wiley, New York, 1977), Vols. I and II.
[39] A. Giusti-Suzor, X. He, O. Atabek, and F. H. Mies, Phys. Rev. Lett. **64**, 515 (1990).